VOL. 18, NO. 20, OCTOBER 2023 ISSN 1819-6608
ARPN Journal of Engineering and Applied Sciences
©2006-2023 Asian Research Publishing Network (ARPN). All rights reserved.
www.arpnjournals.com

DESIGN AND OPTIMIZATION OF CHITOSAN-ALGINATE NANOPARTICLES FOR PLANT GROWTH HORMONE INDOLE-3-ACETIC ACID

Narissara Kulpreechanan[1], Krittiya Singcharoen[2], Soontree Khunthong[3], Methee Juntaropakorn[3] and Feuangthit N. Sorasitthiyanukarn[4]
[1]Department of Public Health, Faculty of Medicine, Western University Watcharapol Campus, Pathum Thani, Thailand
[2]Nanoscience and Technology (International Program), Graduate School, Chulalongkorn University, Bangkok, Thailand
[3]Department of Resources and Environment, Faculty of Science at Sriracha, Kasetsart University Sriracha Campus, Chon Buri, Thailand
[4]Center of Excellent in Natural Products for Ageing and Chronic Diseases, Chulalongkorn University, Bangkok, Thailand
E-Mail: Feuangthit.n@chula.ac.th

ABSTRACT

Excessive use of agrochemicals can lead to environmental degradation, and thus, a potential solution is to control their release using biodegradable polymeric nanoparticles. This study aimed to fabricate indole-3-acetic acid chitosan/alginate nanoparticles (IAA-CANPs) through o/w emulsification and ionotropic gelation, employing a Box-Behnken design (BBD) to evaluate the influence of various factors (alginate: chitosan mass ratio (ALG:CS), Tween™ 80, and IAA concentration) on particle size, zeta potential, and encapsulation efficiency (EE). Response surface methodology (RSM) was used to determine the optimum conditions for nanoparticle fabrication, which were ALG:CS mass ratio of 1:0.10, Tween™ 80 of 1.5% w/v, and IAA of 15 mg/mL. The IAA-CANPs produced under these optimal conditions exhibited an average particle size of 275 ± 19 nm, a polydispersity index (PDI) of 0.37 ± 0.9, a zeta potential of -23.8 ± 0.8 mV, and an EE of 68.5 ± 1.4%. The IAA-CANPs also demonstrated superior physico-chemical stability under UV irradiation exposure compared to free IAA. The IAA-CANPs had stability up to 3 months at 4°C. The release pattern in dissolution media at pH 5.5 and 7.5 indicated a sustained-release behavior, which fit well with the Peppas-Sahlin kinetic model, indicating anomalous diffusion, a non-Fickian diffusion mechanism. These findings suggest that CANPs could be a promising approach for encapsulating and controlling the release of IAA, exhibiting excellent physicochemical stability and potential for agricultural applications.

Keywords: chitosan, alginate, nanoparticles, indole-3-acetic acid, controlled release.

Manuscript Received 13 May 2023; Revised 30 November 2023; Published 30 December 2023

1. INTRODUCTION

Agriculture is a crucial economic activity globally, and it is expected to receive an investment of 2.9 billion dollars by 2030. Agrochemicals such as fertilizers, pesticides, and plant growth regulators (PGRs) play a vital role in enhancing agricultural productivity [1]. However, their extensive use can lead to permanent environmental damage and the development of plant pathogen resistance, requiring new agrochemicals or increased dosages of existing ones [2]. Nanoparticle encapsulation is a useful technique to protect and control the release of agrochemicals such as fertilizers, pesticides, herbicides, fungicides, and PGRs [3, 8]. Biodegradable polymers like alginate, cellulose, cyclodextrin, dextran, and chitosan are commonly used to synthesize nanoparticles for this purpose [4]. Chitosan (CS) and alginate (ALG) are natural biopolymers that have gained attention as potential delivery systems for agrochemicals due to their biodegradability, biocompatibility, and safety [1, 5]. Alginate is a natural polymer extracted from brown algae, composed of α-L-guluronic acid and β-d-mannuronic acid. It is stable under acidic conditions but dissolves in alkaline environments. Alginate has the potential for encapsulating bioactive compounds, enabling their controlled release in acidic or neutral alkaline environments [6]. Alginate nanoparticles are formed via ionotropic gelation with divalent cations or cationic polymers [7-8]. However, these nanoparticles tend to be unstable at room temperature, which can cause the encapsulated compounds to leak out of the nanoparticle matrices [9-10]. Nevertheless, chitosan, a cationic polysaccharide produced by deacetylating chitin, can be used to stabilize alginate nanoparticles [7, 11-12]. CANPs have been used as carriers for various active ingredients in agriculture, such as insecticides such as cartap hydrochloride [13] and acetamiprid [8], herbicides like imazapic and imazapyr [1], and micro-nutrients like copper oxide nanoparticles [16]. However, there have been limited studies on their effectiveness as a release system for plant growth regulators (PGRs).Chitosan/alginate nanoparticles (CANPs) have found diverse applications in agriculture, particularly as carriers for encapsulating and delivering various active ingredients, such as insecticides like cartap hydrochloride and acetamiprid, herbicides like imazapic and imazapyr, and micro-nutrients like copper oxide nanoparticles [4, 2]. Although previous research has highlighted the potential of CANPs as a delivery matrix for various molecules, there have been limited studies on their effectiveness as a release system for plant growth regulators (PGRs). PGRs are a group of natural or

©2006-2023 Asian Research Publishing Network (ARPN). All rights reserved.

synthetic compounds that mimic the behavior of plant hormones, acting at low concentrations to modulate plant growth and development. These compounds are commonly used in agriculture to improve crop yields, enhance product quality, and induce plant responses to stress. Examples of PGRs include auxins, cytokinins, gibberellins, ethylene, abscisic acid, brassinosteroids, and nitric oxide [1]. Auxin, such as indole-3-acetic acid (IAA), is an important plant growth regulator that controls various aspects of plant development. However, the application of PGRs like auxin in agriculture is challenging due to their susceptibility to environmental stress [14-15]. To overcome this, CANPs loaded with different PGRs have been developed for controlled release [16-18]. These nano-encapsulated PGRs have shown increased effectiveness in promoting plant growth and development. Design of experiment (DOE) approaches, such as Box-Behnken design (BBD) and response surface methodology (RSM), have been used by researchers to assess the impact of parameters such as size, surface charge, morphology, and physicochemical properties of the encapsulated active compounds on the release of active compounds from CANPs. Studies have shown the effectiveness of these approaches in evaluating the influence of variables on the release of active compounds [4, 19-21].

In this study, RSM and BBD were utilized to examine the influence of alginate: chitosan mass ratio (ALG:CS), Tween™ 80, and IAA concentration on the fabrication of CANPs loaded with IAA (IAA-CANPs). The optimal conditions were determined and used to obtain the IAA-CANPs, which were characterized using various instrumental techniques. The release of IAA from the CANPs was also studied, and the physicochemical stability of the IAA-CANPs was evaluated.

2. MATERIALS AND METHOD

2.1 Materials

Sodium alginate (ALG), with a molecular weight range of 80,000-120,000 g/mol and a guluronic acid content of 0.39, was procured from Sigma located in St. Louis, MO, USA. Chitosan (CS), having a molecular weight of 75,000 g/mol and a deacetylation degree of 85%, was provided by Marine Bio Resources Co., Ltd. in Samut Sakorn, Thailand. Tween™ 80 was acquired from Thermo Fisher ACROS Organics™ situated in Geel, Belgium. Indole-3-Acetic acid (IAA) (99% purity was purchased from Loba Chemie™ Pvt. Ltd. (Mumbai, India). Analytical grade chemicals were used for the experiment, and purified water was obtained through the Milli-Q® water purifier manufactured by Millipore, France.

2.2 Preparation of IAA-CANPs

To prepare the IAA-CANPs, the oil in water (o/w) emulsification and ionotropic gelification methods described by Sorasitthiyanukarn *et al*. [22] were used with some modifications. Initially, different concentrations of ethanolic IAA solution were added dropwise into 20 mL of alginate solution (0.6 mg/mL, pH 4.9) containing different concentrations of Tween™ 80 under continuous magnetic stirring at 1000 rpm for 10 min. The resulting mixture was then sonicated for 15 min using an ultrasonic bath. Next, 4 mL of $CaCl_2$ solution (0.67 mg/mL) was slowly added and continuously stirred for 30 min. The resulting emulsion was mixed with 4 mL of chitosan solution (pH 4.6) at various ALG:CS mass ratios and stirred for an additional 30 min. The resulting suspension was then equilibrated overnight in the dark at room temperature, and the IAA-CANPs were obtained as a dispersion in an aqueous solution.

2.3 Design and Optimization of IAA-CANPs

The Box Behnken statistical design (BBD) was employed to create various nanoparticle formulations. Three factors, namely the ALG:CS mass ratio (X_1), Tween™ 80 (X_2), and IAA concentrations (X_3), were considered, each with three different levels (low, medium, and high). Three responses were also evaluated, including particle size (Y_1), zeta potential (Y_2), and encapsulation efficiency (EE) (Y_3). Table-1 summarizes the factors and their respective levels, as well as the responses.

Table-1. Factors and responses in BBD for preparation of IAA-CANPs.

	Level used		
	Low	**Medium**	**High**
Factors			
X_1 = ALG:CS	1:0.15	1:0.125	1:0.10
X_2 = Tween™ 80 (% w/v)	1	2	3
X_3 = IAA (mg/mL)	5	10	15
Responses	Constraints		
Y_1 = Particle size (nm)	Minimize		
Y_2 = Zeta potential (mV)	$Y_2 \geq \pm 20$		
Y_3 = EE (%)	Maximize		

Using Design Expert software® version 13 (Stat-Ease, Inc., Minneapolis, MN, USA), a total of 15 experimental runs were generated, as shown in Table-2. In order to assess the interaction effects of factors in the nanoparticle formulations, a 3-factor, 3-level BBD was utilized. Using the results obtained from the experimental runs shown in Table-2, a polynomial model was generated for each response. These models were calculated using the Design Expert software® and are presented below.

$$Y_n = \beta_0 + \beta_1X_1 + \beta_2X_2 + \beta_3X_3 + \beta_{12}X_1X_2 + \beta_{13}X_1X_1 + \beta_{23}X_2X_3 + \beta_{11}X_1^2 + \beta_{22}X_2^2 + \beta_{33}X_3^2 \quad (1)$$

where β_0 is intercept, β_1, β_2 and β_3 are linear coefficients β_{12}, β_{13}, and β_{23} are interaction coefficients while β_{11}, β_{22}, and β_{33} are quadratic coefficients.

©2006-2023 Asian Research Publishing Network (ARPN). All rights reserved.

Table-2. Observed responses in BBD for development and optimization of IAA-CANPs.

Run	factor			Response		
	X_1	X_2	X_3	Y_1	Y_2	Y_3
1	1:0.10	1	10	303 ± 19	-25.9 ± 0.5	52 ± 3.2
2	1:0.15	1	10	516 ± 22	-19.8 ± 1.1	62 ± 4.5
3	1:0.10	3	10	441 ± 17	-22.6 ± 0.8	57 ± 2.7
4	1:0.15	3	10	541 ± 13	-16.9 ± 1.3	62 ± 3.8
5	1:0.10	2	5	265 ± 28	-24.2 ± 0.7	35 ± 2.6
6	1:0.15	2	5	426 ± 15	-18.8 ± 1.5	50 ± 2.3
7	1:0.10	2	15	309 ± 23	-21.3 ± 0.8	66 ± 1.6
8	1:0.15	2	15	470 ± 26	-16.6 ± 1.3	59 ± 2.8
9	1:0.125	1	5	404 ± 11	-20.6 ± 1.9	36 ± 1.2
10	1:0.125	3	5	478 ± 13	-18.2 ± 1.2	46± 3.5
11	1:0.125	1	15	424 ± 24	-19.3 ± 0.9	70 ± 2.9
12	1:0.125	3	15	524 ± 31	-15.3 ± 1.5	63 ± 1.8
13*	1:0.125	2	10	438 ± 21	-16.1 ± 1.1	70.1 ± 2.2
14*	1:0.125	2	10	421 ± 16	-17.1 ± 1.4	68 ± 3.4
15*	1:0.125	2	10	447 ± 28	-15.8 ± 0.2	70 ± 1.6

* Indicates the center point of the design.

2.4 Characterization

The dynamic light scattering (DSL) technique was utilized to measure the particle size and polydispersity index (PDI). The zeta potential was measured using Laser Doppler Micro-electrophoresis on a Zetasizer, Nano-ZS instrument (Malvern Instruments Worcestershire, Ltd., UK). The morphology of the nanoparticles was studied by Transmission Electron Microscopy (TEM) using a JEM 1400 Plus instrument (JEOL, Tokyo, Japan). To determine EE, the supernatant of the IAA-CANPs suspension was collected after ultracentrifugation at 4°C, 35,000 rpm for 45 min using a Hitachi Ultracentrifugation (Model CP100-NX, Hitachi Koki, Tokyo, Japan). The amount of free IAA in the supernatant was determined using a UV-Vis spectrophotometer at 280 nm. The values of EE were calculated using the following equation.

$$EE\ (\%) = [(W_i - W_s)/W_i] \times 100 \quad (2)$$

where W_i and W_s are the total amounts of initial IAA and the total amount of IAA in supernatant.

2.5 Release Kinetics Assays and Mathematical Modeling

To evaluate the release of IAA from IAA-CANPs, a dialysis bag diffusion technique was employed with modifications based on a previously reported protocol by Ana Valderrama *et al*. [23]. The releasing medium consisted of water containing 30% ethanol, adjusted to pH 5.5 and 7.5, which is a commonly used pH range in plant hormone studies due to its optimal range for many enzymes involved in plant hormone metabolism and signaling pathways. Ethanol was added to increase IAA solubility and promote uniform release while minimizing aggregation [23-24]. Both the IAA-CANP suspension and free IAA solution, at an equivalent IAA concentration, were loaded into the dialysis bags and incubated at ambient temperature with continuous gentle shaking at 100 rpm. At specific time intervals (0-96 h), 2-mL aliquots were withdrawn from the releasing medium and quantified for IAA amount using UV-vis spectrophotometry at 280 nm. An equivalent amount of the releasing medium was immediately replenished to maintain sink conditions and promote drug diffusion into the surrounding medium. The release data were modeled using the DDSolver program in Excel, and the release kinetics were evaluated using various statistical parameters, including $R^2_{adjusted}$, Akaike information criterion (AIC), and model selection criterion (MSC). The selection of the best-fitted kinetic model was based on the highest $R^2_{adjusted}$ and AIC values, as well as the lowest MSC values [36].

2.6 Physicochemical Stability Study of IAA-CANPs

2.6.1 Photostability

The photostability of IAA-CANPs was evaluated following the protocol reported by Li et al. [37], with some modifications. In brief, 20 mL of both IAA solution (free IAA) and IAA-CANP suspension were placed in clear bottles and were exposed to UV lamp irradiation

©2006-2023 Asian Research Publishing Network (ARPN). All rights reserved.

environments (30 W, 254 nm) for 1 h. The distance between the samples and the UV lamp was kept constant at 26 cm. Sampling was taken at specific intervals, and the amount of IAA in both free IAA and IAA-CANPs was analyzed using UV–vis spectrophotometry at 280 nm. The percentage of IAA remaining after the test was calculated using Eq. (3).

IAA retention (%) = (IAA at each time interval / IAA at initial) × 100 (3)

2.6.2 Storage stability

The stability of IAA-CANP suspension during storage was evaluated for a period of 3 months at two different temperatures, 4°C and 25°C [38]. The IAA-CANP suspension was stored in amber colored vials and kept in a refrigerator at 4°C or in a cabinet at room temperature (25°C). The physicochemical properties of the IAA-CANPs, including particle size, zeta potential, and EE, were analyzed at specific time intervals using the same method as previously described.

2.7 Statistical Analysis

All experiments in this study were conducted in triplicate and results were expressed as means ± standard deviation (SD). Data were analyzed using Microsoft Excel 365 (Microsoft Corporation) and statistical analyses were performed using one-way analysis of variance (ANOVA) for comparisons between groups, and t-tests for comparisons within groups. A p-value of less than 0.05 was considered statistically significant.

3. RESULTS AND DISCUSSIONS

3.1 Statistical Analysis of the BBD

Based on the experimental results obtained using the BBD model, it was observed that the nanoparticles exhibited an average size (Y_1), zeta potential (Y_2), and EE (Y_3) value within the range of 265 ± 28 to 541 ± 13 nm, -15.3 ± 1.5 to -25.9 ± 0.5 mV, and 36.3 ± 1.2% to 70.1 ± 1.6%, respectively (Table-2). Furthermore, regression equations were formulated to elucidate the relationship between the independent variables and the response variables, as represented by Eqs (4) - (6), respectively.

Table-3. Summary of results of regression analysis for all responses.

Response	*p*-value	R^2	$R^2_{adjusted}$	$R^2_{predicted}$	Lack of fit	Remark
Response (Y_1): Particle size						
Linear	0.0016	0.7367	0.6648	0.4420	0.0636	-
2FI	0.7333	0.7737	0.6039	-0.1801	0.0497	-
Quadratic	< 0.0001	0.9952	0.9865	0.9755	0.9060	Suggested
Factors that have a statistically significant effect on the response Y_1 ($p < 0.05$) are X_1, X_2 และ X_3						
Response (Y_2): Zeta potential						
Linear	0.0089	0.6372	0.5383	0.4068	0.0745	-
2FI	0.9857	0.6434	0.3760	-0.1264	0.0512	-
Quadratic	0.0002	0.9905	0.9735	0.9338	0.7968	Suggested
Factors that have a statistically significant effect on the response Y_2 ($p < 0.05$) are X_1 , X_2 และ X_3						
Response (Y_3): EE						
Linear	0.0196	0.5782	0.4632	0.3093	0.0158	-
2FI	0.4402	0.6935	0.4635	0.2610	0.0145	-
Quadratic	0.0004	0.9902	0.9725	0.8636	0.2193	Suggested
Factors that have a statistically significant effect on the response Y_3 ($p < 0.05$) are X_1, X_2 และ X_3						

Particle size (Y_1) $= + 435.4 + 79.25X_1 + 41.92X_2 + 19.33X_3 – 28.33X_1X_2 + 0.0001X_1X_3 + 6.15X_2X_3 - 37.58X_1^2 + 52.39X_2^2 - 30.31X_3^2$ (4)

Zeta potential (Y_2) $= - 16.29 + 2.75X_1 + 1.57X_2 + 1.18X_3 – 0.12X_1X_2 - 0.18X_1X_3 + 0.42X_2X_3 – 3.43X_1^2 - 1.55X_2^2 - 0.49X_3^2$ (5)

EE (Y_3) $= + 69.38 + 3.17X_1 + 1.06X_2 + 11.19X_3 – 1.48X_1X_2 - 5.70X_1X_3 - 4.43X_2X_3 – 6.09X_1^2 - 5.25X_2^2 – 10.32X_3^2$ (6)

The above equation revealed that the primary factor with a statistically significant effect ($p < 0.05$) on the size (Eq. 4) and zeta potential (Eq. 5) of the nanoparticles was the ALG: CS (X_1), which demonstrated a positive effect. Additionally, the concentration of IAA

©2006-2023 Asian Research Publishing Network (ARPN). All rights reserved.

was identified as the primary factor with a statistically significant effect ($p < 0.05$) on the EE of the nanoparticles, also showing a positive effect. It has been observed that an increase in the ALG: CS ratio results in an increase in nanoparticle size, which may be attributed to an increase in the thickness of the CS layer surrounding the nanoparticles. Consequently, larger nanoparticles are formed [25]. Moreover, an excessive concentration of Tween^{TM} 80 in the system beyond a certain threshold can result in the aggregation of unstable clusters due to the overloading of Tween^{TM} 80 molecules, caused by an increase in system viscosity. Consequently, the concentration of Tween^{TM} 80 in the system may be considered a parameter that can lead to an increase in nanoparticle size [26]. Conversely, it was found that the concentration of IAA in the system does not exhibit any significant statistical correlation ($p > 0.05$) with nanoparticle size. However, an increase in the concentration of IAA may lead to an interaction between IAA and the polymer, resulting in an increase in system viscosity, which can lead to the formation of larger nanoparticles. Interestingly, it was observed that increasing the CS component in the ALG:CS ratio resulted in a decrease (more positive) in the zeta potential value of the nanoparticles. This may be attributed to the protonation of the carboxylate group (CH_3COO-) of ALG by the positively charged amino group (NH_3^+) in the chemical structure of CS. This protonation results in a decrease in the negative charge of the zeta potential [26]. Furthermore, increasing the concentrations of both Tween^{TM} 80 and IAA in the system led to a decrease in the negative zeta potential value of the nanoparticles. This phenomenon may be attributed to the increase in system viscosity, which causes the formation of larger and less stable nanoparticle aggregates, resulting in a decrease in the negative zeta potential value [27]. Eq. (6) suggests that the concentration of IAA plays a critical role in enhancing EE of nanoparticles, as evidenced by its higher coefficient compared to other factors. The study revealed that the EE value of nanoparticles increases with increasing concentration of IAA. This could be attributed to the concentration gradient that exists between the IAA solution and the enlarged surface area of the nanoparticles, which enhances the rate of diffusion of IAA into the nanoparticles, thereby increasing the amount of IAA encapsulated inside [26-27]. Furthermore, increasing the concentration of IAA may increase its binding to the surface of the nanoparticles, resulting in higher retention of IAA inside the nanoparticles. This is because IAA molecules that bind to the surface of the nanoparticles are unable to diffuse out into the surrounding fluid. These factors collectively contribute to an increase in the EE value of the nanoparticles [28]. Moreover, an increase in the proportion of CS in ALG:CS ratio also enhances the EE value. This could be due to the thicker CS layer that covers the ALG nanoparticles, thereby minimizing the leakage of IAA trapped inside the nanoparticles [29-30]. Additionally, an increase in the concentration of Tween^{TM} 80 also leads to higher EE values. This may be attributed to the appropriate concentration of Tween^{TM} 80 in the system, which helps to emulsify the process better, leading to improved stability and integrity of the nanoparticles, thus resulting in an increase in the EE value. Moreover, the ANOVA analysis performed on the experimental data of nanoparticle size, CS concentration, and EE demonstrated that all factors exhibited R^2 and $R^2_{predicted}$ values above 86% (Table 3). These results suggest that the experimental data were well-fitted to the model and can be utilized to describe the association between the factors and response. Furthermore, the model can be employed to forecast the most suitable formulation for the synthesis of nanoparticles.

©2006-2023 Asian Research Publishing Network (ARPN). All rights reserved.

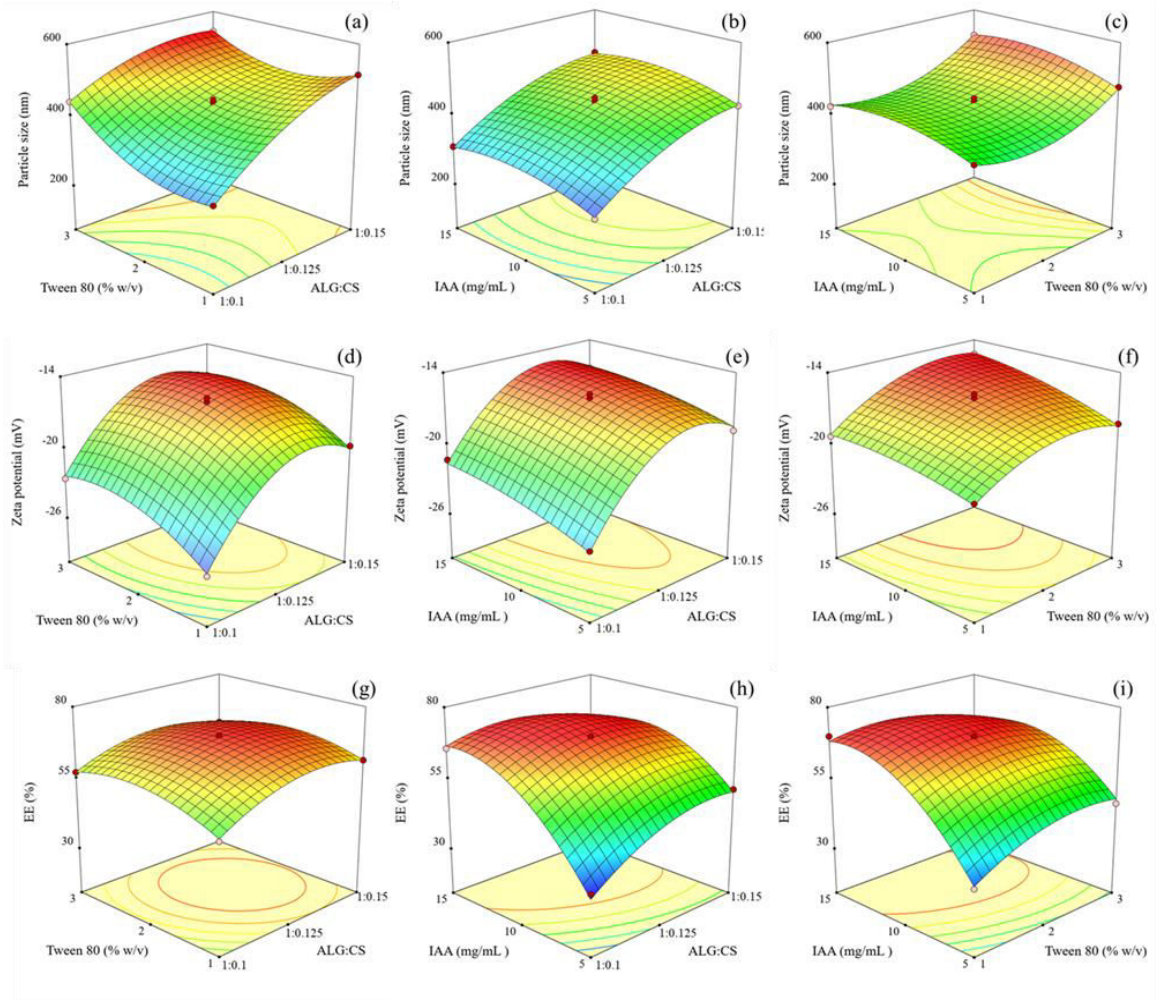

Figure-1. 3D-Response surface plots showing the effects of investigated factors on: (a-c) particle size (Y_1), (d-f) zeta potential (Y_2), (e-f) and EE (Y_3).

3.2 Optimization and Model Validation

The optimal condition for preparing nanoparticles was determined using Design Expert® statistical software. The numerical optimization technique and the desirability function were utilized to determine the optimal formulation with the maximum desirability value. The optimal formulation was defined as having the smallest particle size, zeta potential > ± 20, V, and the highest EE value, as presented in Table-4. The statistical prediction results indicated that the optimal formulation for preparing nanoparticles consisted of an ALG:CS of 1:0.10, a Tween™ 80 concentration of 1.5% (w/v), and an IAA concentration of 15 mg/mL. The predicted response values for particle size, CS concentration, and EE were 283 nm, -22.9 mV, and 66.4%, respectively. Subsequently, the nanoparticles prepared using the optimal formulation were analyzed to determine their characteristics. A comparison was then made between the predicted values and the actual experimental results to calculate the percentage error. Statistical analysis revealed no significant difference (p > 0.05) between the predicted and experimental values, suggesting that the predicted values obtained from the software can be considered as actual values for the preparation of nanoparticles.

Table-4. Optimized condition of IAA-CANPs with experimental observed and predicted values.

Factor	Optimum	Response	Predicted	Observed	% Error
ALG:CS mass ratio	1:0.10	Particle size (nm)	283	275 ± 19	-2.9
Tween™ 80 (%w/v)	1.5	Zeta potential (mV)	-22.9	-23.8 ± 0.8	+3.7
IAA (mg/mL)	15	EE (%)	66.4	68.5 ± 1.4	+3.1

Notes: % Error = [(observed value - predicted value) / observed value] x 100. Desirability value was 0.92; The polydispersity index (PDI) value of the optimized formulation was 0.37 ± 0.9

©2006-2023 Asian Research Publishing Network (ARPN). All rights reserved.

3.3 Characterizations

The results of the analysis of the size and morphology of the IAA-CANPs prepared from the optimal formulation using TEM are presented in Figures 2a and 2b. It was observed that the nanoparticles were spherical in shape, with a smooth surface and an average diameter of approximately 200 nm, with good size distribution.

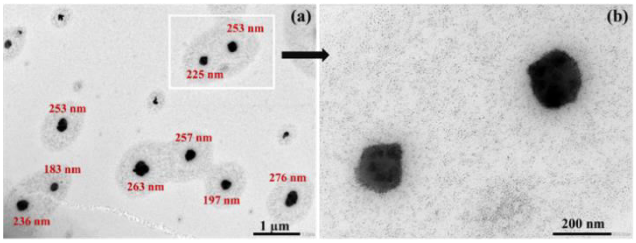

Figure-2. TEM images of (a) size distribution and (b) morphology of IAA-CANPs prepared from the optimal formulation. (Figure-2a is magnified at 8000x and Figure-2b is magnified at 50, 000x).

3.4 Physico-Chemical Stability

3.4.1 Storage stability

The results of a stability study of IAA-CANPs stored at 4°C and 25°C for 90 days are shown in Figures 3(a)-3(c). At 4°C, the size, zeta potential, and EE of the nanoparticles remained statistically unchanged ($p > 0.05$) after 90 days of storage, compared to the initial state. In contrast, at 25°C, the nanoparticles exhibited an increase in size, a decrease in zeta potential, and a decrease in EE after more than 60 days of storage. These findings indicate that storing the nanoparticles at 4°C is more effective in maintaining their stability compared to storage at 25°C.

3.4.2 Light stability

The results of the light stability study of IAA-CANPs and IAA solution under a UV light source simulation for 120 min, as shown in Figure-4(d), revealed that the IAA in the form of a solution degraded rapidly after 60 min of UV exposure. The remaining percentage of IAA (% IAA remaining) was only 42.3 ± 2.7% compared to its initial state, and it continued to decrease over time after UV exposure. The percentage of remaining IAA was less than 5% after 120 min of UV exposure. This study is consistent with the chemical properties of IAA, which has a chemical structure with a conjugated double bond that can quickly degrade when exposed to light, resulting in the formation of reactive free radicals that can degrade or alter the effectiveness of IAA [31]. However, although the degradation of IAA encapsulated in nanoparticles after exposure to UV light was observed, similar to IAA solution, it was found that the percentage of remaining IAA-CANPs was higher than in a solution. The percentage of remaining IAA-CANPs after exposure to UV light for 120 minutes was 27.3 ± 3.3%, which was much higher than that of IAA solution (4.2 ± 2.5%). These findings suggest that the light stability of IAA may increase when it is encapsulated in CANPs, which have the potential to effectively protect IAA from light-induced degradation.

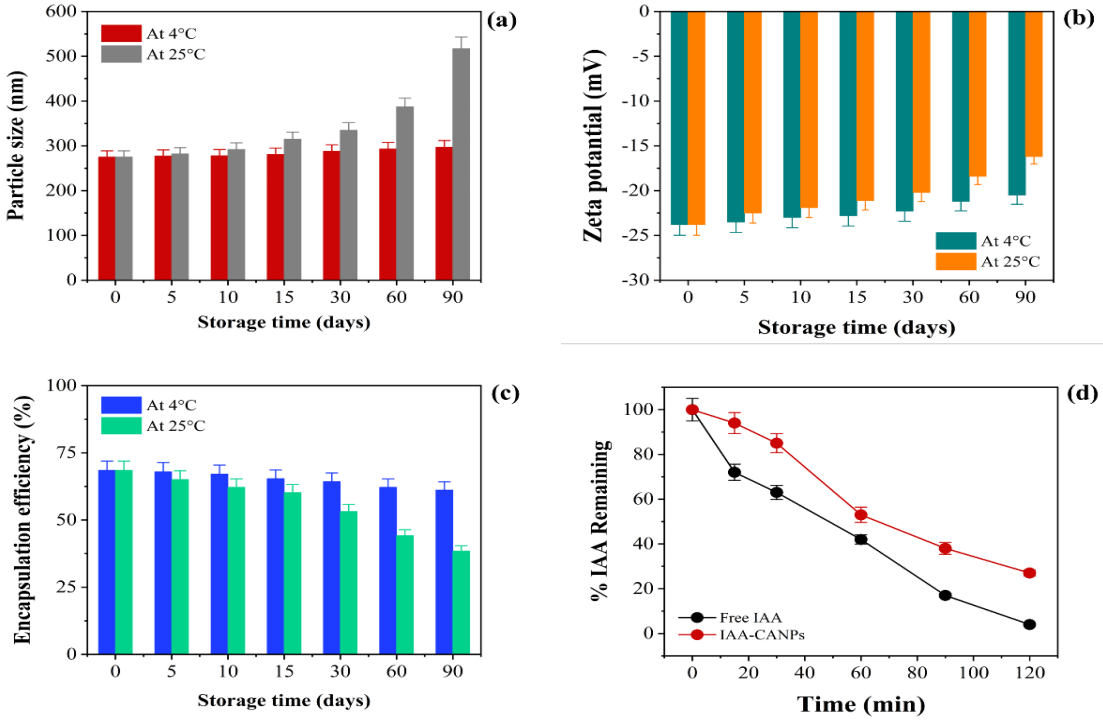

Figure-3. The storage stability of IAA-CANPs is expressed in changes of (a) particle size, (b) zeta potential and (c) EE at 4°C and 25°C for 90 days ($n = 3$); (d) percentages of retention IAA in IAA-ACNPs and IAA solution upon exposure to UV light radiation ($n = 3$).

©2006-2023 Asian Research Publishing Network (ARPN). All rights reserved.

3.5 Release Kinetics Assays and Mathematical Modelling

3.5.1 Release profile of IAA

The release profiles of free IAA and IAA from IAA-CANPs (at an equivalent IAA concentration) were obtained in dissolution media at pH 5.5 and pH 7.5, as shown in Figure-4. The cumulative release profiles of free IAA in both dissolution media showed rapid release in the first 8 h, followed by slow release until 48 h. The release of IAA increased by less than 3.3% during the period of 48 to 96 h, indicating the sustained-release characteristics of free IAA in all dissolution media. On the other hand, IAA was released much slower after being encapsulated within CANPs compared to free IAA. The results suggest the sustained-release manner of IAA-CANPs. For example, after 24 h, 54% and 35% of IAA were released from IAA-CANPs in dissolution media at pH 5.5 and 7.5, respectively. In contrast, more than 70% of free IAA was released in the two-dissolution media.

Additionally, the results indicated that the release of IAA from IAA-CANPs was more prominent under acidic conditions (pH 1.2) than slightly alkaline conditions (pH 7.5). The increased release in acidic conditions was attributed to the high solubility of CS in acidic environments, which facilitated the leakage of the encapsulated IAA through the porous structure of the CANPs into the dissolution media [32]. In contrast, the release of IAA from the IAA-CANPs was reduced in neutral or alkaline environments due to the shrinkage of chitosan, which hindered the release of the encapsulated IAA from the nanoparticles [32]. These findings suggest that IAA-CANPs have the potential to be used as a controlled and sustained-release delivery system for IAA.

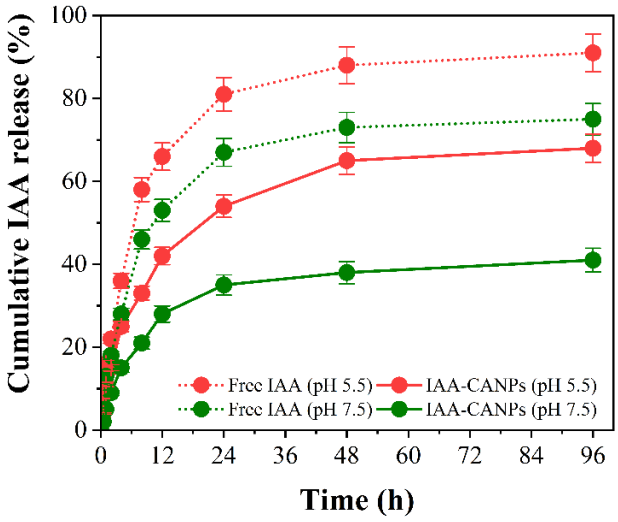

Figure-4. Percentage of cumulative release of free IAA and IAA from IAA-CANPs in dissolution media at pH 5.5 and pH 7.5, respectively.

3.5.2 Release kinetic of IAA from IAA-CANPs

The kinetic model fitting results presented in Table-4 demonstrate that the Peppas-Sahlin model had the highest $R^2_{adjusted}$ and MSC values, and the lowest AIC values for the release profile of IAA from IAA-CANPs in both pH 5.5 and pH 7.5 dissolution media. This model combines Fickian diffusion (controlled by diffusion) and non-Fickian release (relaxation of the nanoparticle matrix). The Peppas-Sahlin model's release exponent (m) value indicates the type of diffusion mechanism: a value less than 0.45 indicates Fickian diffusion, while $0.45 < m < 0.85$ indicates non-Fickian diffusion [33-34]. The IAA release exponent (m) value in both pH 5.5 (0.563) and pH 7.5 (0.589) dissolution media was greater than 0.45 but less than 0.85, suggesting that IAA release occurs through anomalous diffusion, which is a non-Fickian diffusion mechanism. To further explore the contribution of nanoparticle matrix relaxation and compound diffusion phenomena, the diffusion constant (k_1) and relaxation constant (k_2) of the Peppas-Sahlin model were compared. A higher value of k_1 than k_2 indicates that drug diffusion is more important than the relaxation of the nanoparticle matrix, whereas a higher value of k_2 than k_1 implies that nanoparticle matrix relaxation is the dominant contributor [35]. As per the values presented in Table 4, compound diffusion is the major contributor to IAA release from IAA-CANPs in both pH 5.5 and pH 7.5 dissolution media. Therefore, the release of IAA from IAA-CANPs in both dissolution media is likely to occur through two mechanisms: (1) Fickian diffusion, which is governed by the concentration gradient of the compound between the nanoparticles and the dissolution media, and (2) non-Fickian diffusion or anomalous transport, which is caused by the erosion of the nanoparticle matrix.

©2006-2023 Asian Research Publishing Network (ARPN). All rights reserved.

Table-4. Kinetic modeling on IAA released from IAA-CANPs by DDSolver.

Model	Evaluation criteria						
	Media	$R^2_{adjusted}$	AIC	MSC	k_n	n	m
Zero-order ($F = k_0.t$)	pH 5.5	0.241	85.432	-0.121	0.964	-	-
	pH 7.5	0.199	76.489	-0.170	0.583	-	-
First-order ($F = 100.\ e^{-k_1 t}$)	pH 5.5	0.739	74.781	0.945	0.031	-	-
	pH 7.5	0.418	73.301	0.149	0.009	-	-
Hixson-Crowell ($F = 100.[1-(1-k_{HC}.t)^3]$)	pH 5.5	0.639	78.051	0.618	0.009	-	-
	pH 7.5	0.345	74.490	0.031	0.003	-	-
Korsmeyer-Peppas ($F = k_{KP}.t^n$)	pH 5.5	0.943	60.339	2.389	0.350	15.384	-
	pH 7.5	0.914	54.959	1.982	0.344	9.623	-
Higuchi ($F = k_H.t^{0.5}$)	pH 5.5	0.639	78.051	0.618	0.009	-	-
	pH 7.5	0.834	60.761	1.403	5.330	-	-
Peppas-Sahlin ($F = k_1.\ t^m + k_2.\ t^m$)	pH 5.5	0.998	36.611	4.762	k_1 = 11.461 k_2 = -0.471	-	0.563
	pH 7.5	0.981	40.415	3.437	k_1 = 7.128 k_2 = -0.299	-	0.589

4. CONCLUSIONS

In this study, the fabrication and optimization of IAA-CANPs were successfully achieved through the application of BBD and RSM, resulting in the desired characteristics of the nanoparticles. The morphology of the optimized IAA-CANPs appeared spherical and exhibited a narrow size distribution. Moreover, the optimized IAA-CANPs demonstrated better physicochemical stability against UV irradiation compared to free IAA and exhibited promising storage stability for up to 3 months at 4°C. The release profile of IAA from the optimized IAA-CANPs showed a sustained-release pattern following the Peppas-Sahlin kinetic model, indicating anomalous diffusion, which is a non-Fickian diffusion mechanism. These results suggest that CANPs hold great potential as delivery systems for IAA, serving as an alternative plant hormone for agricultural applications.

ACKNOWLEDGMENTS

This study was financially supported by the Kasetsart University Sriracha Campus (fiscal year 2022), Thailand, and the authors expressed their gratitude for the funding. The Research Fund of Western University, Thailand, is also acknowledged for their support.

Conflict of Interest

The authors declare no conflict of interest.

REFERENCES

[1] Maruyama C. R., Guilger M., Pascoli M., Bileshy-Jose N., Abhilash P. C., Fraceto L. F., De Lima R. 2016. Nanoparticles based on chitosan as carriers for the combined herbicides imazapic and imazapyr. Sci. Rep. 6: 23854.

[2] Malerba M., Cerana R. 2019. Recent Applications of Chitin- and Chitosan-Based Polymers in Plants. Polymers. 11: 839.

[3] Disease G., Maluin F. N., Hussein M. Z., Yusof N. A., Fakurazi S. 2019. Preparation of chitosan - hexaconazole nanoparticles as fungicide nanodelivery system for combating. Molecules 24: 2498.

[4] Choudhary R. C., Kumari S., Budhwar S. 2019. Chitosan nanomaterials for smart delivery of bioactive compounds in agriculture. In: Publishers, C.R.C. (Ed.), Nanoscale Engineering in Agricultural Management, pp. 124-139 (St. Louis, Missouri, USA).

[5] Pereira A. E. S., Silva P. M., Oliveira J. L., Oliveira H. C., Fraceto L. F. 2017. Chitosan nanoparticles as carrier systems for the plant growth hormone gibberellic acid. Colloids Surf. B Biointerfaces. 150: 141-152.

[6] Karim A., Rehman A., Feng J., Noreen A., Assadpour E., Kharazmi M. S., Lianfu Z., Jafari S. M. 2022. Alginate-based nanocarriers for the delivery and controlled-release of bioactive compounds. Adv Colloid Interface Sci. 307: 102744.

©2006-2023 Asian Research Publishing Network (ARPN). All rights reserved.

[7] Niculescu A. G., Grumezescu A. M. 2022 Applications of Chitosan-Alginate-Based Nanoparticles-An Up-to-Date Review. Nanomaterials (Basel). 12: 186.

[8] Kumar S., Chauhan N., Gopal M., Kumar R., Dilbaghi N. 2015. Development and evaluation of alginate-chitosan nanocapsules for controlled release of acetamiprid. Int J Biol Macromol. 81: 631-637.

[9] Setty C. M., Sahoo S. S., Sa B. 2005. Alginate-coated alginate-polyethyleneimine beads for prolonged release of furosemide in simulated intestinal fluid. Drug Dev Ind Pharm. 31(4-5): 435-46.

[10] Hassani Najafabadi A., Azodi-Deilami S., Abdouss M., Payravand H., Farzaneh S. 2015. Synthesis and evaluation of hydroponically alginate nanoparticles as novel carrier for intravenous delivery of propofol. J Mater Sci Mater Med. 26: 145.

[11] Li S., Zhang H., Chen K., Jin M., Vu S. H., Jung S., He N., Zheng Z., Lee M.S. 2022. Application of chitosan/alginate nanoparticle in oral drug delivery systems: prospects and challenges. Drug Deliv. 29: 1142-1149.

[12] Almutairi F. M., El Rabey H. A., Alalawy A. I., Salama A. A. M., Tayel A. A., Mohammed G. M., Aljohani M. M., Keshk A. A., Abbas N. H., Zayed M. M. 2021. Application of Chitosan/Alginate Nanocomposite Incorporated with Phycosynthesized Iron Nanoparticles for Efficient Remediation of Chromium. Polymers (Basel). 13: 2481.

[13] Kaur I., Agnihotri S., Goyal D. 2021. Fabrication of chitosan-alginate nanospheres for controlled release of cartap hydrochloride. Nanotechnology. 33: 025701.

[14] Woodward A. W., Bartel B. 2005. Auxin: regulation, action, and interaction. Ann Bot. 95: 707-35.

[15] Korpayev S., Karakeçili A., Dumanoğlu H., Ibrahim Ahmed Osman S. 2021. Chitosan and silver nanoparticles are attractive auxin carriers: A comparative study on the adventitious rooting of microcuttings in apple rootstocks. Biotechnol J. 8: e2100046.

[16] Kudasova D., Mutaliyeva B., Vlahoviček-Kahlina K., Jurić S., Marijan M., Khalus S. V., Prosyanik A. V., Šegota S., Španić N., Vinceković M. 2021. Encapsulation of Synthesized Plant Growth Regulator Based on Copper (II) Complex in Chitosan/Alginate Microcapsules. Int. J. Mol. Sci. 22: 2663.

[17] Pereira A. D. E. S., Oliveira H. C., Fraceto L. F. 2019. Polymeric nanoparticles as an alternative for application of gibberellic acid in sustainable agriculture: a field study. Sci Rep. 9: 7135.

[18] Vlahoviček-Kahlina K., Jurić S., Marijan M., Mutaliyeva B., Khalus S. V., Prosyanik A. V., Vinceković M. 2021. Synthesis, Characterization, and Encapsulation of Novel Plant Growth Regulators (PGRs) in Biopolymer Matrices. Int. J. Mol. Sci. 22: 1847.

[19] Abdel-Hafez S. M., Hathout R. M., Sammour O. A., 2014. Towards better modeling of chitosan nanoparticles production: screening different factors and comparing two experimental designs. Int. J. Biol. Macromol. 64: 334-340.

[20] Sorasitthiyanukarn F. N., Muangnoi C., Gomez C. B., Suksamrarn A., Rojsitthisak P., Rojsitthisak P. 2023. Potential Oral Anticancer Therapeutic Agents of Hexahydrocurcumin-Encapsulated Chitosan Nanoparticles against MDA-MB-231 Breast Cancer Cells. Pharmaceutics. 15: 472.

[21] Sorasitthiyanukarn F. N., Muangnoi C., Thaweesest W., Bhuket P. R. N., Jantaratana P., Rojsitthisak P., Rojsitthisak P. 2020. Polyethylene Glycol-Chitosan Oligosaccharide-Coated Superparamagnetic Iron Oxide Nanoparticles: A Novel Drug Delivery System for Curcumin Diglutaric Acid. Biomolecules. 10: 73.

[22] Sorasitthiyanukarn F. N., Ratnatilaka Na Bhuket P., Muangnoi C., Rojsitthisak P., Rojsitthisak P. 2019. Chitosan/alginate nanoparticles as a promising carrier of novel curcumin diethyl diglutarate. Int. J. Biol. Macromol. 131: 1125-1136.

[23] Ana Valderrama N., Christian Jacinto H., Lay J., Yoselyn Flores, E., Daniel Zavaleta C., Alfredo Rodríguez D. 2020. Factorial design for preparing chitosan nanoparticles and its use for loading and controlled release of indole-3-acetic acid with effect on hydroponic lettuce crops. Biocatal. Agric. Biotechnol. 26: 101640.

[24] Riekes M. K., Kuminek G., Rauber G. S., Cuffini S. L., Stulzer H. K. 2104. Development and Validation of an Intrinsic Dissolution Method for Nimodipine Polymorphs. Cent Eur. J. Chem. 12: 549-556.

©2006-2023 Asian Research Publishing Network (ARPN). All rights reserved.

[25] Bhunchu S., Rojsitthisak P., Rojsitthisak P. 2015. Effects of preparation parameters on the characteristics of chitosan-alginate nanoparticles containing curcumin diethyl disuccinate. J. Drug Deliv. Sci. Technol. 28: 64-72.

[26] Sharma N., Madan P., Lin S. 2016. Effect of process and formulation variables on the preparation of parenteral paclitaxel-loaded biodegradable polymeric nanoparticles: A co-surfactant study. AJPS. 11: 404-416.

[27] Sukmawati A., Utami W., Yuliani R., Da'I M., Nafarin A. 2018. Effect of tween 80 on nanoparticle preparation of modified chitosan for targeted delivery of combination doxorubicin and curcumin analogue. IOP Conf. Ser.: Mater. Sci. Eng. 311: 012024.

[28] Katas H., Raja M. A., Lam K. L. 2013. Development of Chitosan Nanoparticles as a Stable Drug Delivery System for Protein/siRNA. Int. J. Biomater. 2013: 146320.

[29] Sarmento B., Ribeiro A. J., Veiga F., Ferreira D. C., Neufeld R. J. 2007. Insulin-loaded nanoparticles are prepared by alginate ionotropic pre-gelation followed by chitosan polyelectrolyte complexation J. Nanosci. Nanotechnol. 7: 2833-2841.

[30] Kiaie N., Aghdam R. M., Tafti S. H. A., Emami S. H. 2016. Statistical Optimization of Chitosan Nanoparticles as Protein Vehicles, Using Response Surface Methodology. J. Appl. Biomater. Funct. Mater. 14: 413-422.

[31] Leasure C. D., Chen Y. P., He Z. H. 2013. Enhancement of indole-3-acetic acid photodegradation by vitamin B6. Mol. Plant. 6: 1992-1995.

[32] Sorasitthiyanukarn F. N., Muangnoi C., Ratnatilaka Na Bhuket P., Rojsitthisak P. Rojsitthisak P. 2018. Chitosan/alginate nanoparticles as a promising approach for oral delivery of curcumin diglutaric acid for cancer treatment. Mater. Sci. Eng. C. 93: 178-190.

[33] Siepmann J., Peppas N. A. 2012. Modelling of Drug Release from Delivery System Based on Hydroxypropyl Methylcellulose (HPMC). Adv. Drug Del. Rev. 64: 163-174.

[34] Peppas N. A., Sahlin J. J. 1989. A simple equation for description of solute release III. Coupling of Diffusion and Relaxation. Int. J. Pharm. 57: 169-172.

[35] Khushbu Jindal R. 2022. Thermal Stability and Optimization of Graphene Oxide Incorporated Chitosan and Sodium Alginate Based Nanocomposite Containing Inclusion Complexes of Paracetamol and β-Cyclodextrin for Prolonged Drug Delivery Systems. Polym. Bull. 80: 1751-1772.

[36] Zhang Y., Huo M., Zhou J., Zou A., Li W., Yao C., Xie S. 2010. DDSolver: An Add-in Program for Modeling and Comparison of Drug Dissolution Profiles. AAPS J. 12: 263-271.

[37] Li M., Zahi M. R., Yuan Q., Tian F., Liang H. 2016. Preparation and Stability of Astaxanthin Solid Lipid Nanoparticles Based on Stearic Acid. Eur. J. Lipid Sci. Technol. 118: 592-602.

[38] ICH Q1A(R2) International Conference on Harmonization (ICH). 2003. Guidance for Industry: Q1A(R2) Stability Testing of New Drug Substances and Products. Ich Harmon. Tripart. Guidel. 4: 24.